



HAL
open science

Rare earth and alkali elements in stalagmites, as markers of Mediterranean environmental changes during Termination I

L. Drugat, E. Pons-Branchu, Éric Douville, L. Foliot, L. Bordier, M. Roy-Barman

► To cite this version:

L. Drugat, E. Pons-Branchu, Éric Douville, L. Foliot, L. Bordier, et al.. Rare earth and alkali elements in stalagmites, as markers of Mediterranean environmental changes during Termination I. *Chemical Geology*, 2019, 525, pp.414-423. 10.1016/j.chemgeo.2019.08.001 . hal-02457924

HAL Id: hal-02457924

<https://hal.science/hal-02457924>

Submitted on 21 Jun 2021

HAL is a multi-disciplinary open access archive for the deposit and dissemination of scientific research documents, whether they are published or not. The documents may come from teaching and research institutions in France or abroad, or from public or private research centers.

L'archive ouverte pluridisciplinaire **HAL**, est destinée au dépôt et à la diffusion de documents scientifiques de niveau recherche, publiés ou non, émanant des établissements d'enseignement et de recherche français ou étrangers, des laboratoires publics ou privés.

1 Rare earth and alkali elements in stalagmites, as markers of

2 Mediterranean environmental changes during Termination I.

3

4

5 L. Drugat, E. Pons-Branchu, E. Douville, L. Foliot, L. Bordier, M. Roy-Barman

6 Laboratoire des Sciences du Climat et de l'Environnement, LSCE/IPSL, CEA-CNRS-UVSQ, Université Paris-
7 Saclay, F-91191 Gif-sur-Yvette, France

8

9 Keywords: Speleothem, alkali metals, rare earth elements, Termination I, Mediterranean,
10 environmental changes

11

12

13

14 ABSTRACT

15 Speleothems represent a key source of information on climate variations in continental
16 environments as they enable high temporal resolution reconstructions. The stalagmite salam3
17 presented in this study comes from the Salamandre Cave (SE France, Gard region). Its growth period,
18 determined by $^{230}\text{Th}/^{234}\text{U}$ chronology and MOD-AGE extrapolation, falls between 10.91 ± 1.00 kyr BP
19 and 13.43 ± 0.25 kyr BP, which corresponds to the transition between the last glacial period and the
20 Holocene. This period is essential for the understanding of past and future climate variations.

21 In this study, trace elements were measured along the growth axis of this stalagmite and
22 results were compared with the elementary composition of bedrock and soil above the cave. Three
23 periods were identified with high Li, Rb, Cs, Th and rare earth element (REE) concentrations, between
24 13.43 ± 0.25 and 13.11 ± 0.27 , between 12.70 ± 0.34 and 12.30 ± 0.15 kyr, and between 11.31 ± 0.86
25 and 11.15 ± 0.87 kyr.

26 Our results suggest that the alkali metals (alkalis) studied are either associated in the detrital phase
27 with the clay and particle fraction (correlation with Th), or with the organic matter and colloids as
28 complexed ligands (correlation with Mn). To attribute the origin of REE measured within the
29 stalagmite, we compared their pattern with those of soil and bedrock, and two sources were deduced:
30 i) periods with an enrichment in light REE and no cerium anomaly corresponding to mobilization from
31 soil during weathering episodes such as the Bölling-Alleröd period; ii) from bedrock during a longer
32 residence time of water in the epikarst such as during the Younger Dryas and the Holocene. Thus, as
33 illustrated in this study, combined analysis of REE and alkalis can provide key information on soil
34 weathering linked to climate/ environmental change.

35

36

37

38 1. INTRODUCTION:

39 In recent decades, particular attention has been paid to the comprehension of stable isotopes ($\delta^{18}\text{O}$ and
40 $\delta^{13}\text{C}$) in speleothems. Despite their major contributions to climate studies, the interpretation of stable
41 isotopes remains challenging because several factors (kinetic fractionation, evaporation, water source,
42 etc.) can affect their variations, and their use as climate proxies varies strongly depending on the site
43 studied. Trace elements (TE) within speleothems have also been intensively studied in recent years
44 and have proved to be useful for paleoclimatic reconstructions. To date, Mg and Sr are most
45 commonly used as hydrological proxies (e.g. Fairchild et al., 2000; Fairchild & Treble, 2009;
46 Hellstrom & McCulloch, 2000; Bourdin et al., 2011; Rutledge et al., 2014 ; Ünal-Imer et al., 2016).
47 A recent study by Owen et al., 2016 showed that Mg/Ca could be affected by a change in source
48 composition, which makes it difficult to use as a tool for the reconstruction of hydrologic processes.
49 They highlight the need to use Ca isotopes to quantify these mechanisms and avoid problems due to
50 variable source composition or detrital contamination. In the same vein, our study could help
51 disentangle the interactions in the soil zone that affect trace element concentrations before their
52 transfer to the epikarst system.

53 Improving our knowledge of the parameters driving trace element concentration changes within
54 speleothems is crucial for climate and environmental studies. These parameters include drip water
55 chemistry, the source of these elements and weathering processes, but also incorporation mechanisms
56 within CaCO_3 crystals (Bourdin et al., 2011). Trace elements can come from local sources such as soil
57 or host rock weathering or from an exogenous source such as aeolian dust or marine spray (Goede et
58 al., 1998; Frumkin and Stein, 2004). Rare earth elements (REE) or some of the alkalis such as Li, Cs
59 and Rb are still poorly studied in speleothems (Zhou et al., 2008, 2012; Bourdin et al., 2011).

60 The present study focused on these poorly studied trace elements, specially alkalis, within a
61 speleothem from SE France (salam3), that recorded the Termination I period, which was characterized
62 by rapid changes in climatic (including precipitation) conditions, in order to determine the sensitivity
63 of these tracers. Very few speleothem records from this specific climatic period in Europe have been

64 studied so far (e.g. Genty et al., 2006; Moreno et al., 2010), mainly because in many mid-latitude
65 locations, climatic conditions were not favorable to speleothem growth.

66 Termination I is a strategic period for paleoclimatic studies as it is chronologically defined
67 between 18.0 kyr BP and 11.0 kyr BP (Kasper et al., 2014) and includes the Heinrich event 1, the
68 oldest Dryas, the Bölling period, the older Dryas, and the Younger Dryas. Termination I is of great
69 interest as it is the link between the last glacial termination and the onset of deglaciation, which
70 corresponds to the current interglacial period, the Holocene (Kasper et al., 2014). It is essential to
71 study the Termination I in order to better understand the natural mechanisms controlling climate
72 changes from a glacial period to a warmer one, here the Holocene.

73 The major goal of this study was to explore the possibility of using selected trace elements,
74 namely alkalis and rare earth elements, in speleothems as geochemical tracers for the paleo-
75 reconstruction of hydrological and soil processes. We first characterize the relationships between these
76 elements and the cross-information that they can provide on source, transport and uptake processes.
77 We then situate these processes in the framework of the climate variability observed during the
78 Termination I around the Mediterranean region, in order to determine soil weathering phases, periods
79 of vegetation change, and differences in the transport and sources of these trace elements. These
80 observations are finally compared with other European archives (speleothems, lakes and pollens) in
81 order to place the stalagmite salam3 in the particular climatic context of the different phases of the
82 Termination I.

83

84 **2. STUDY CONTEXT:**

85 **2.1. Geological setting**

86 The Salamandre cave is located in SE France, northwest of the Méjannes-Le-Clap plateau, at
87 44°13' N 4°21' E in the Cèze valley. It is formed of Barremian limestone with Urgonian facies over
88 730 m for a gradient of 89 m. This fossil network consists of a 45 m access shaft opening into a vast
89 gallery with small E-W side galleries, which are old fossil hydraulic conduits. This cave was

90 previously studied in an attempt to determine the origin of the collapse of some very large pillars
91 (Pons-Branchu, et al., 2004).

92 The Salamandre record will be compared with different archives, speleothems or lakes located in
93 Europe (Figure 1).

94

95 **Figure 1 (Google Earth image): Yellow dots are the sites used for climate comparison. 1: Chauvet cave, Genty et al.,**
96 **2006; 2: Meerfelder Maar lake, Brauer et al., 2008; 3: ODP-976, Chabaud et al., 2014. Red dot: Salamandre cave**

97

98 **2.2. Site characteristics:**

99 Today, the Salamandre cave site is characterized by a Mediterranean climate, with hot dry summers
100 and strong irregular rainfall especially during autumn. At Aubenas, 58 km from the studied cave, the
101 annual average precipitation between 2006 and 2016 was ~ 924 mm (website infoclimat
102 <https://www.infoclimat.fr/climatologie/annee/2016/aubenas/valeurs/07570.html>) and the mean annual
103 temperature during this 10-year period was around 13.5 °C.

104 Today the soil above the cave is terra rossa soil, typical of the Mediterranean region, and is less than
105 15 cm thick. The vegetation is scrubland with bush and green oaks.

106 The cave is located around 80 km north of the Mediterranean coast, at a latitude of ca 44° N. This area
107 is particularly interesting in order to study the atmospheric circulation changes between the low and
108 high latitudes for the Holocene (Magny et al., 2013).

109

110 **3. MATERIAL AND METHODS**

111 Salam3 is a 75.5 centimeter-long stalagmite. The general color of the stalagmite is beige with some
112 orange or whitish areas. X ray diffraction measurements on several samples along the growth axis
113 showed that it can be characterized as pure calcite. Bedrock and soil samples were also collected
114 above the cave.

115

116 3.1. U-Th analysis and dating

117 Between 200 and 350 mg of calcite were cut for each sample. They were dissolved with hydrochloric
118 acid in beakers in which a triple spike (^{229}Th , ^{233}U and ^{236}U) had been previously added. After iron co-
119 precipitation, uranium and thorium fractions were separated and purified using a U-teva resin
120 (Eichrom technology) in nitric media. Details about U-Th separation and purification can be found in
121 (Pons-Branchu, et al., 2014). U and Th isotopic compositions were then analyzed on the multi-
122 collector inductively coupled plasma mass spectrometer (MC-ICP-MS) Neptune Plus ^{ThermoScientific} fitted
123 with a jet interface and an aridus 2 desolvating system, at the Laboratoire des Sciences du Climat et de
124 l'Environnement (LSCE), Gif s/Yvette, France. To correct U and Th mass fractionation, we used the
125 exponential law (normalized to the $^{238}\text{U}/^{235}\text{U}$ isotope ratio of 137.88, Cowan and Adler, 1976) and
126 standard/sample bracketing.

127 ^{230}Th and ^{234}U (and for a few samples ^{229}Th) were measured on the axial electron multiplier, in
128 jumping mode, while ^{229}Th , ^{232}Th , ^{233}U , ^{236}U , ^{235}U and ^{238}U were measured on Faraday cups. In order
129 to measure all the isotopes during the same sequence, U and Th fractions were mixed in sufficient
130 proportions to be able to measure the signal at mass 229 and 233 between 2 and 30 mV and ^{238}U
131 between 3 and 15 V on a Faraday cup (see Pons-Branchu et al., 2014 for details).

132

133 3.2. Trace element analysis

134 139 samples were collected along the growth axis of salam3 stalagmite, 7 samples were collected
135 from the bedrock (1.1, 1.2, 2.1, 2.2, 3.1, 3.2 and 4.2) and 2 from the soil. For the stalagmite and
136 bedrock 3 to 7 mg of powder of each sample were carefully extracted using a stainless steel micro drill
137 with a diamond tip. Trace-grade HNO_3 and Milli-Q water were systematically used for dissolutions
138 and dilutions.

139 3.2.1. *CaCO₃ samples:*

140 The samples were dissolved in 0.5N HNO₃ and diluted to obtain solutions containing 100 ppm of
141 calcium. Finally, they were centrifuged in order to eliminate particles that can plug the nebulizer (e.g.
142 clays). The analyses were performed at LSCE, Gif s/Yvette, France using a Quadrupole ICP-MS (ICP-
143 QMS) Xseries^{II Thermo Scientific}. The analytical protocol was based on the standard addition method for
144 Ca-100 ppm solutions at 0.5 N HNO₃ (Rosenthal et al., 1999; Harding et al., 2006; Bourdin et al.,
145 2011).

146 *Measured isotopes:*

147 ⁷Li, ²⁵Mg, ⁴³Ca, ⁴⁴Ca, ⁴⁸Ca, ⁵⁵Mn, ⁸⁵Rb, ⁸⁸Sr, ⁸⁹Y, ¹³³Cs, ¹³⁹La, ¹⁴⁰Ce, ¹⁴¹Pr, ¹⁴⁶Nd, ¹⁴⁷Sm, ¹⁵⁷Gd, ¹⁵⁹Tb,
148 ¹⁶³Dy, ¹⁶⁵Ho, ¹⁶⁸Er, ¹⁶⁹Tm, ¹⁷²Yb, ¹⁷⁵Lu, ²³²Th, ²³⁸U.

149 An in-house standard at Ca-100 ppm was analyzed every 10 samples to correct the long-term drift of
150 the ICP-QMS for each mass. All the samples were analyzed in a random order, trace element
151 concentrations and their associated uncertainties (2 σ , 95% of confidence) were verified and validated
152 by analyzing three SRM (registered trademark of the National Institute of Standards and Technology)
153 carbonates referenced: JCp-1 (aragonite coral), Jct-1 (aragonite giant clam) and calcite BAM (Bourdin
154 et al., 2011)(Case, Robinson, Auro, & Gagnon, 2010), Gerard Aalbersbergb, Carole Be'geota et al.,
155 2006). The relative precision was 1–3 % for alkalis and uranium, 5 % for Y and Mn and about 10 %
156 for REE within CaCO₃ (bedrock and stalagmite).

157 3.2.2. Soil samples

158 For the two soil samples, the preparation and analyses were done at the SARM laboratory, and the
159 complete method is detailed in (Carignan et al., 2001). Uncertainties for each element correspond to
160 the relative standard deviation of the mean. The majors were analyzed on an ICP-AES and the trace
161 and rare earth elements on an ICPMS iCAP-Q^{Thermo Scientific}. Measurement precision was between 5 and
162 15% depending on the elements considered.

163

164 4. RESULTS

165 4.1. Chronology

166

167 The uranium (^{238}U) concentrations ranged between 0.136 ± 0.001 and 0.180 ± 0.001 ppm, while the
168 ^{232}Th concentrations ranged between 1.302 ± 0.010 and 17.09 ± 0.14 ppb (see table 1). The $^{230}\text{Th}/^{232}\text{Th}$
169 ratio ranged from 4.36 ± 0.04 to 48.09 ± 0.32 . Ages are reported as kyr BP “before 1950”. For age
170 determination, a classical correction for initial ^{230}Th using ($(^{230}\text{Th}/^{232}\text{Th}) = 1.5 \pm 50\%$) was first
171 applied, then a second one, using stratigraphic correction (Hellstrom, 2006) with the StrutAge routine
172 (Roy-Barman and Pons-Branchu 2016). 2839 valid results were obtained with the Monte Carlo
173 simulations of StrutAge and defined a $^{230}\text{Th}/^{232}\text{Th}$ initial activity ratio ($(^{230}\text{Th}/^{232}\text{Th})_0$) of 1.23 ± 0.07 . The
174 chronological model (depth-ages) was constructed using the MOD-AGE software (Hercman &
175 Pawlak, 2012) and the corrected ages obtained with the StrutAge routine, giving modelled ages from
176 top to base of the speleothem for each 0.5 mm. These ages were used to determine growth rates, with
177 the highest rate (1.26 to 0.40 mm per yr) at the beginning of the sequence, between 13.43 ± 0.25 kyr
178 BP and 12.52 ± 0.26 kyr BP, and the lowest rate (0.02 mm per yr), between 12.33 ± 0.09 kyr and
179 11.59 ± 0.65 kyr (Figure 2). Large error bars on the youngest ages are due to the high detrital content
180 for these levels. The growth period of salam3 covers the Bölling-Alleröd period, the Younger Dryas
181 and the very beginning of the Holocene (Figure 2). The initial $\delta^{234}\text{U}$ ($\delta^{234}\text{Ui}$) values depended on the
182 growth periods: between 94.42 ± 1.42 and 72.37 ± 0.96 ‰ for the oldest period, until 12.71 kyr BP \pm
183 0.33 , and between 64.54 ± 1.33 and 66.63 ± 0.92 ‰ for the youngest period (from 12.52 kyr BP \pm
184 0.26 to the top).

185

186 4.2. Trace elements

187

188 The 139 samples analyzed cover a time period of 2530 years, and a mean temporal resolution
189 of 20 years. Trace element variations in the salam3 stalagmite display contrasted variations (Figure 3).

190 Three main periods of high alkalis, namely Li, Rb, and Cs (called alkalis here) content, are
191 specifically outlined. Period 1 (between 13.43 ± 0.25 and 13.11 ± 0.27 kyr BP during the Bölling-
192 Alleröd), is characterized by a high content of alkalis and Th, a maximum growth rate but extremely
193 low content of REE and Mn. Periods 2 and 3 are characterized by a high content of both alkalis, Th
194 and REE and occur respectively between 12.70 ± 0.34 and 12.30 ± 0.15 kyr BP (during the Younger
195 Dryas) and at the beginning of the Holocene, from 11.31 ± 0.86 kyr BP.

196

197 4.2.1 Alkali metals and Th

198 In salam3, alkali concentrations display a large variation range, namely from 18 to 488 ppb for Li, 22
199 to 952 ppb for Rb and 2 to 88 ppb for Cs. To our knowledge, very few studies have dealt with alkali
200 contents in speleothems. Among them, Li concentrations ranged from 24 to 470 ppb in speleothems
201 from two Israeli caves (von Strandmann et al., 2017) and water from Ballynamintra cave in Ireland
202 had Rb concentrations of 0.85 ppb and Cs concentrations of 0.07 ppb (Baldini et al., 2012).

203 There is a very good correlation between the three alkalis studied: the R^2 for Cs and Li is 0.93 and 0.92
204 for Rb and Li (see figure A1a and A1b in Supplementary material), and to a lesser extent between
205 these alkalis and Th: $R^2 \approx 0.7$ (see figure A1c in Supplementary material). The mean concentrations
206 measured in stalagmite, bedrock and soil are summarized in Table 3.

207

208 4.2.2 Rare earth elements

209 In salam3, the total REE concentrations vary from 15 to 1628 ppb (mean concentration: 207 ppb), La
210 vary from 2.47 to 257 ppb (mean concentration: 39 ppb) and Lu from 0.04 to 6.28 ppb (mean
211 concentration: 0.86 ppb). In the nearby Chauvet cave, the REE concentrations were much lower (total
212 REE ranging from 24 to 125 ppb, La ranging from 4.7 to 22 ppb and Lu ranging from 0.17 to 0.69
213 ppb, Bourdin et al., 2011). By contrast, the Songja cave (China) displays La concentrations between 4
214 and 570 ppb, and Lu concentrations between 0.6 and 4.5 ppb (Zhou et al., 2008).

215 The stalagmite REE concentrations are averaged for the three climatic periods considered (see table 3
216 with Bölling-Alleröd: BA, Younger Dryas: YD, and Holocene: HO).

217 In the bedrock, the REE concentrations vary by a factor of 6. These mean REE concentrations were ca
218 25 times higher than those of the stalagmite.

219 In soil samples, the total REE concentrations were around 40 times higher than those of the bedrock
220 and around 1000 times higher than in the stalagmite.

221 The REE concentrations in salam3, in the bedrock and in the soil were normalized to the North
222 American Shale Composite (NASC) concentrations (Gromet et al., 1984) in order to smooth the
223 concentration variations that are not related to Earth surface processes (Bourdin et al., 2011) (Figure
224 4).

225 For the bedrock samples, the NASC normalized REE pattern displays a negative Ce anomaly (Ce*).

226
$$Ce^* = (2 * Ce) / (La + Pr)$$

227 For the two soil samples, as REE concentrations were homogeneous, the mean concentration was
228 used. The patterns do not display a Ce anomaly but an enrichment in LREE (light rare earth elements
229 which include the REE from La to Gd) compared to HREE (heavy rare earth elements which include
230 the REE from Gd to Yb). The BA pattern displays a different shape from that of the YD and the HO,
231 with no Ce anomaly (Ce*=0.90) and a relatively flat pattern. The REE patterns corresponding to YD
232 and HO are similar to that of the bedrock, with a Ce negative anomaly (Ce*= 0.74 and 0.79
233 respectively) and a depletion in LREE.

234

235 **5. DISCUSSION**

236 **5.1. Origin and incorporation of the trace elements**

237 Different factors can affect the trace element concentration variations within speleothems such as
238 temperature, rainfall, trace element concentrations and speciation in the sources, water residence time,
239 growth rate and kinetic of incorporation. Variation in vegetation cover is also a major parameter, as
240 organic matter plays an important role in the transport of some trace elements due to carrier phases

241 (e.g. Gascoyne 1983; Roberts et al., 1998; Fairchild et al., 2000; Zhou et al., 2008; Bourdin et al.,
242 2011; Hartland et al., 2012; Zhou et al., 2012).

243 The significance of these factors or processes affecting trace element contents in the cave dripwater
244 and trace element incorporation varies with the studied site (climate, geometry of the karst, thickness
245 and nature of soil, etc.). For example, the role of climate on trace element variation is very different
246 from one site to another, and can also vary for a single site with changing conditions over time
247 (Schimpf et al., 2011).

248 For Salamandre cave, the following sections discuss incorporation processes, source variation and
249 weathering intensity for alkalis, rare earth elements, thorium and manganese.

250

251 5.1.1. Sources of alkali metals

252 The strong correlation observed between Li, Rb and Cs (fig A1) suggests a common behavior and
253 mechanism of transport and/or incorporation affecting these three elements or common sources. The
254 mean content of Li, Rb and Cs in the bedrock is two to five times lower than in the stalagmite, and soil
255 concentrations are 500 to 1500 times higher than in the stalagmite (Table 3).

256 While the low alkali contents in the speleothem are close to the bedrock composition, the Cs vs Rb
257 diagram allows the identification of two potential sources of alkalis (Figure 5), the first one being the
258 bedrock. Cs is known to be found in soil and sediments and to have a great affinity with the clay
259 fraction (Kisakürek, et al., 2004; Tanaka & Watanabe, 2015). This suggests that the second source is
260 linked to the weathering of silicate and/or an exogenous source (atmospheric flux for instance).

261 Alkalis are known to be very mobile during alteration and weathering processes (e.g. Palmer and
262 Edmond 1989; Kisakürek et al., 2004; Millot et al., 2010), but the correlation ($R^2 = 0.7$) and link
263 between alkalis and Th suggests that at least part of the alkalis are bound on particulate or colloidal
264 matter, as shown for other elements such as Al or Fe (Belli et al., 2017). The inputs of alkalis
265 congruently dissolved from the bedrock and the soil of the Salamandre site are represented as strait
266 mixing lines (Figure 5). The Cs-Rb trend is different between the BA period and the HO-YD periods
267 (different regression lines).

269 In order to better constrain the alkali sources and transport mode, one of the alkalis (Cs) was
270 normalized to two different less mobile elements (Figure 6): Th that traces clay minerals and Mn that
271 is carried by organic matter and colloids (Zhou et al., 2008). During BA, the Cs/Mn ratio is highly
272 variable and the Cs/Th ratio is low, implying that Cs is better correlated to Th, and suggesting a Cs
273 association with clay/soil inputs (Th rich). During YD and HO, the Cs/Mn ratio is low and the Cs/Th
274 ratio is highly variable, implying that Cs is better correlated to Mn than to Th, suggesting a Cs
275 association with carrier phases of organic matter or colloids.

276

277

278 5.1.2. Sources and transportation of rare earth elements

279 In karst systems, the REE sources and their conditions of transport or incorporation into the calcite of
280 speleothems are still poorly documented. Their main sources are commonly assumed to be the bedrock
281 and the soil (e.g. Zhou et al., 2008; Fairchild & Treble, 2009) but the climatic significance of their
282 concentration change or trend is still not totally understood.

283 In most cases, when the REE are associated with manganese and increase during warm and wet
284 periods, this is related to enhanced weathering from soil or bedrock (e.g. Richter et al., 2004; Zhou et
285 al., 2008; Pazand & Javanshir, 2013). In other cases, it has been suggested that their incorporation rate
286 is controlled by a crystallographic process and growth rate kinetics which are driven by climate
287 (Bourdin et al., 2011).

288 In the Salamandre cave, the REE pattern of the soil displayed an enrichment in light rare earth
289 elements (LREE) and no Ce anomaly (Figure 4). The bedrock patterns show a weak Ce anomaly and a
290 LREE depletion. In first assumption, this difference between bedrock and soil can help to distinguish
291 the source signature in the salam3 stalagmite. In water-carbonate interaction, LREE and HREE have
292 not the same transport mechanism: HREE are known to be complexed by carbonate ions and
293 transported as soluble complexes bonded with fulvic acids and/or organic ligands, whereas LREE are

294 more associated with and stabilized by particles such as metal-oxides and colloids (e.g. Elderfield et
295 al., 1990; Sholkovitz, 1992; Tanizaki et al., 1992; Zhou et al., 2008; Bourdin et al., 2011).

296 Consequently, the LREE/HREE (normalized to the NASC) ratio can help us to illustrate the
297 fractionation between these two groups. In the soil, the ratio is about 0.93 and in the bedrock 0.69. In
298 *salam3*, this ratio is higher during the BA (0.76) than during the YD and HO (respectively 0.56 and
299 0.55), confirming a higher contribution of the soil during BA as was observed with the alkali elements
300 (section 5.1.1).

301 A second assumption can be made concerning the different origin of REE for BA on one hand and YD
302 and HO in the other hand. As underlined in figure 4, the REE trend for the YD and HO periods is
303 similar to the bedrock REE pattern, and the REE trend for the BA period is not enriched in HREE and
304 could include a new source such as Saharan dust, a common component of terra rossa Mediterranean
305 soils (e.g. Merino & Banerjee, 2008; Erel & Torrent, 2010), with no HREE enrichment (e.g. Muhs et
306 al., 2007). The direct contribution of such aerosols inside the cave due to ventilation changes appears
307 to be excluded here due to the configuration of the cave and the speleothem location. African dust
308 deposited on soil above the cave could however impact stalagmite composition. A recent study on
309 Greenland dust detected a contribution of Saharan dust toward the northern direction at the BO-YD
310 transition but not before (Han et al., 2018). The Mediterranean marine record (Box et al., 2008)
311 suggests a significant dust input during the H1 event, but not during the following BA period. In the
312 Aliborean sea, Rodrigo-Gámiz et al. (2011) suggested that the BA and YD periods display no
313 difference in dust input, while during the period between 11.65 to 10.00 kyr cal BP, the marine records
314 increase slightly in eolian input. Bout-Roumazielles et al. (2013) also reported a high African eolian
315 input in the Mediterranean region during BA and YD. Thus, the hypothesis of a higher input of
316 Saharan aerosols during the BA has to be rejected, but the history of the soil above the cave can be
317 inherited from long term African dust/aerosol inputs. As, the BA is a wet climatic period, the
318 deposition of these aerosols in the soil was doubtless prior to the BA, during a period when conditions
319 were more arid, a mechanism suggested by Carolin et al., 2018.

320 5.1.3. Redox sensitive elements

321 Mn, Ce and U are 3 redox sensitive elements. Combining these elements could give some insight into
322 the redox conditions in the soil and during the transport of these elements. Mn exists as soluble Mn^{2+}
323 under reducing conditions and insoluble Mn^{4+} that precipitates as MnO_2 under oxidizing conditions.
324 Similarly, Ce exists as soluble Ce^{3+} under reducing conditions and insoluble Ce^{4+} that precipitates as
325 CeO_2 under oxidizing conditions. In addition to Mn, Ce oxidation can be traced by the Ce-anomaly
326 that represents the deviation of Ce^{4+} compared to the other REE (REE^{3+} only). However, the
327 development of a Ce anomaly can be suppressed when organic ligands are present (Pourret et al.,
328 2008). In contrast to Mn and Ce, U exists as insoluble U^{4+} under reducing conditions and soluble U^{6+}
329 that is stabilized as UO_2^{2+} in solution by carbonate complexes. This contrasting behavior between U
330 and Mn could appear at odds with the good correlation between these two elements (Figure 7).
331 However, it must be kept in mind that U (like other trace elements) has a great affinity for Mn oxides
332 that can serve as the carrying phase for U (Riedel & Kübeck, 2018; Yang et al., 2018).

333 We also observed that during the BA, when REE appear to come preferentially from the soil, there is
334 no Ce anomaly in the speleothem (as in the soil) and during YD and HO, when REE come
335 preferentially from the bedrock, there is a slight negative Ce anomaly in the speleothem (as in the
336 bedrock). These similarities suggest a lack of additional Ce fractionation compared to the other REE
337 and are consistent with the sources already defined based on alkalis and LREE/HREE.

338

339 The comparison between the U isotope data measured for age determination and for trace element
340 characterization is not straightforward due to the different time resolution and sample size.

341 Nevertheless, it can be noted that the systematic decrease in $\delta^{234}\text{U}$ between BA and HO (Figure 7) is
342 also consistent with U coming from 2 sources:

- 343 - a source with a high $\delta^{234}\text{U}$ during BA obtained by leaching of insoluble minerals from the soil (and
344 U^{234} enrichment due to alpha recoil);

345 - a source with a lower $\delta^{234}\text{U}$ during HO obtained by a more congruent dissolution (leading to less
346 preferential leaching of ^{234}U) as expected if a large fraction of the U comes from dissolution of the
347 carbonate from the bedrock.

348

349 In summary, REE and alkalis in the salam3 speleothem of Salamandre cave seem to have 2 major
350 sources:

351 - the soil, characterized by high Cs/Rb and LREE/HREE ratios and no Ce anomaly

352 - the bedrock characterized by low Cs/Rb and LREE/HREE ratios and a slight negative Ce anomaly

353

354 **5.2. REE and alkalis and climate contexts**

355 We analyzed how these different phases of high trace element concentration periods occurred
356 in different climatic contexts and we placed this record in a regional context.

357 The growth rate of stalagmites is known to be linked to temperature and humidity variations. We
358 compared our results with both marine and terrestrial records (Figure 8). The Bölling-Alleröd is a
359 warm and wet period in southern Europe, especially for the Mediterranean area. This is well illustrated
360 by the high percentage of Mediterranean forest pollens in ODP976 (Chabaud et al., 2014), the low
361 $\delta^{13}\text{C}$ at the Chauvet cave (Genty et al., 2006) and in our study by the high growth rate of salam3
362 stalagmite.

363 The Younger Dryas is a cold period from the last glacial maximum (LGM). It is described in
364 many areas around the world in the northern and southern hemispheres and identified in different
365 records: ice cores in Greenland (Severinghaus et al., 1998), chironomid assemblages and sedimentation
366 rates in European lake sediments (Heiri & Millet, 2005; Neugebauer et al., 2012), palynological
367 studies (Allen & Huntley, 2000) or from the evolution of glaciers (Garcia Ruiz et al., 2016).

368 The Younger Dryas in Europe is assumed to have been a mainly cold and dry period, but some studies
369 have described regional variabilities. For example, two phases occur in the Rehwiese lake in Germany,

370 one from 12.67 to 12.27 kyr BP and a cooler one from 12.27 to 11.69 kyr BP (Neugebauer et al.,
371 2012), in the Lautrey lake in Switzerland (Vanni re et al., 2004) or at the La Garma cave in Spain
372 (Baldini et al., 2015). A tripartition of the Younger Dryas is recognized in European lakes, with
373 alternations of drier and wetter periods identified with lake level changes (Lotter, 1992; Magny, 2001;
374 Guiter et al., 2005; Magny et al., 2006).

375 In the salam3 record, the first part of the Younger Dryas (from ca 12.70 to 12.30 kyr BP) is still wet
376 judging from the high growth rate but the second part (from 12.30 to 11.70 kyr BP) is very different
377 with a drastic decrease in the growth rate down to 0.02 mm/yr (Figure 8). The second period of high
378 alkalis that we considered occurred in this first part of the YD, i.e. a still relatively wet but colder
379 period.

380 Finally, the third period with high alkalis occurred during the Holocene which has recently been
381 shown to be a rather unstable period, with various short time variations. Around 11.20 kyr BP, the Pre-
382 boreal oscillation is one of these variations observed in different archives but not homogeneous in
383 terms of climate response (Magny et al., 2007). In salam3, it can be identified by a decrease in the
384 growth rate after a slight increase but due to the low temporal resolution, any conclusions about the
385 growth rates during this period can only be tentative. Thus, the different climatic phases are well
386 recorded in salam3 and show that the three periods with high alkali content discussed above occurred
387 in different climatic conditions.

388

389 5.2.1. Effect of climate on alkalis

390 From the Cs/Mn vs Cs/Th diagram (Figure 6), two different sources were identified, one during the
391 BA and the other during HO and YD.

392 Soil as the main source for the first period with high alkali content, during the warm BA (high
393 stalagmite growth rate, high pollen % in ODP976, low $\delta^{13}\text{C}$ in Chauvet cave, see figure 8), consistent
394 with soil leaching during humid periods.

395 Transport with organic matter during the second and third periods of high alkali content. The
396 mechanism involved could be the same as the one that causes organic matter enrichment and
397 associated bounded-elements (e.g. alkalis elements) in stalagmite laminae during flushing
398 events during fall season (see for instance Baldini et al., 2012). This is consistent with climate
399 and vegetation degradation as recorded for instance by: i) the $\delta^{13}\text{C}$ of Chauvet cave which displays an
400 abrupt increase at the beginning of the YD, interpreted as a rapid vegetation degradation due to colder
401 conditions (Genty et al., 2006); ii) the increase in the varve thickness (enhanced detrital and
402 siliciclastic input) at Meerfelder lake (Brauer et al., 2008); iii) a decrease in the percentage of
403 Mediterranean pollens in the ODP976 record due to drier and colder conditions (Chabaud et al., 2014).
404 The increase in Mn, contemporaneous of the second period of high alkalis (beginning of the YD) in
405 salam3 reflects this vegetation change that enhanced organic matter and colloid mobilization. For the
406 third peak, the preboreal oscillation displays the same tendency in regional climate records, associated
407 with a vegetation degradation.

408

409

410 **6. CONCLUSION**

411 Among the trace elements, rare earth elements and alkalis have seldom been studied as environmental
412 tracers. In this study, salam3, a stalagmite from SE France, has been dated from 13.43 ± 0.25 to 10.91
413 ± 1.00 kyr, a period that covers the transition between the glacial period and the Holocene. The goal of
414 this study was to determine the sources of these trace elements, describe their behaviour and
415 understand their usefulness for reconstructing past climate. We showed that alkalis were associated
416 with Mn or Th depending on the period considered, and enabled the different sources of these
417 elements to be distinguished. The association of alkalis with Th during warm and wet periods (during
418 the BA) is characteristic of a detrital input through particles and clays from the weathering of soil
419 covering the cave. The association of alkalis with Mn reflects an input of organic matter and colloids
420 after a vegetation degradation during cold and/or dry periods (YD and beginning of the HO) which
421 result in soil deterioration. This is confirmed by the increase in elements characteristic of redox

422 changes (Mn, U and Ce anomaly) at the transition between BA and YD and indicates vegetation
423 degradation.

424 The REE patterns within salam3 are different for the 3 climatic periods: for the BA, the pattern (when
425 normalized to NASC) is flat, similarly to soil composition and there is no Ce anomaly. For the YD and
426 HO the REE pattern of salam3 is similar to that of the bedrock, with a LREE depletion. The low REE
427 content during the BA, when the main REE source is soil, suggests that contrary to alkali metals, they
428 are poorly present within the detrital fraction, whereas their high content during YD, similarly to Mn
429 and alkali metals, suggests that they are transported with organic matter and colloids.

430 Thus, trace elements and rare earth elements could be an alternative way to determine wet/dry
431 conditions, erosion or weathering effects or could help to confirm the environmental interpretation of
432 more conventional proxies such as $\delta^{13}\text{C}$ and $\delta^{18}\text{O}$.

433

434 Acknowledgments:

435 We would like to thank the three anonymous reviewers for their helpful comments on the text.

436 We sincerely thank D. Lelièvre and P Benvengut from the Salamandre cave for access to the cave and
437 to the samples. We are grateful to SARM (Service d'Analyse des Roches et des Minéraux from CRPG
438 Nancy) for soil analysis.

439

440

441

442 **FIGURE CAPTIONS**

443 Figure 1 (Google Earth image): Yellow dots are the sites used for climate comparison. 1: Chauvet
 444 cave, Genty et al., 2006; 2: Meerfelder Maar lake, Brauer et al., 2008; 3: ODP-976, Chabaud et al.,
 445 2014. Red dot: Salamandre cave 4

446 Figure 2: Chronological model of the salam3 speleothem (the squares are $^{230}\text{Th}/^{234}\text{U}$ corrected ages
 447 with the stratigraphic constraints, see text for details). Uncertainties are given at 2σ 8

448 Figure 3: Growth rate a) compared to trace element content of salam3: lithium b), rubidium c), cesium
 449 d), manganese (the dotted line is the data points measured and the full line is the running average) e) ,
 450 thorium f), sum of rare earth elements g). The three climatic periods are represented by the colored
 451 areas (green for Bölling-Alleröd, red for the Younger Dryas and blue for the Holocene). The squares
 452 highlight the three peaks of high alkali and Th content during their respective climatic period. 8

453 Figure 4: REE patterns of bedrock, soil and stalagmite normalized to the NASC..... 11

454 Figure 5: Cs and Rb content in salam3 stalagmite. The soil and bedrock values are plotted in brown
 455 and black lines respectively. Blue dots are data corresponding to the Holocene, red squares for the
 456 Younger Dryas and green triangles for the Bölling-Alleröd. 12

457 Figure 6: Different sources for the alkalis. Blue dots correspond to the Holocene, red squares are the
 458 Younger Dryas and green triangles correspond to the Bölling-Alleröd. The brownish square is the soil
 459 and the black square is the bedrock values..... 13

460 Figure 7: Manganese and Uranium concentrations, Ce anomaly and $\delta^{234}\text{U}$ in salam3. The dashed lines
 461 are the data, the full lines are the running average value 15

462 Figure 8: Comparison of Cs/Mn ratio (a) with salam3 growth rate (b) and regional climatic studies:
 463 $\delta^{13}\text{C}$ in Chauvet cave from Genty et al., 2006 (c); varve thickness in Meerfelder maar, from Brauer et
 464 al., 2008 (d); Mediterranean forest %, in ODP976, from Chabaud et al., 2014 (e). 1, 2 and 3
 465 correspond to periods with high alkali content during the following climatic periods, green Bölling-
 466 Alleröd, red Younger Dryas, blue Holocene. 17

467

468 Table 1: Uranium, Thorium concentrations and isotopic ratios. Uncertainties are given at 2σ . $\delta^{234}\text{U} =$
 469 $\left(\frac{{}^{234}\text{U}}{{}^{238}\text{U}} \right)_{\text{measured}} / \left(\frac{{}^{234}\text{U}}{{}^{238}\text{U}} \right)_{\text{equilibrium}} - 1 \times 1000$, with $\left(\frac{{}^{234}\text{U}}{{}^{238}\text{U}} \right)_{\text{equilibrium}} = 54.89 \times 10^{-6}$ (molar ratio.
 470 Cheng et al., 2013). 7

471 Table 2: ${}^{230}\text{Th}/{}^{234}\text{U}$ ages for salam3 stalagmite. Ages are expressed in kyr BP (before 1950).
 472 Uncorrected ages (first column), corrected ages using $\left(\frac{{}^{230}\text{Th}}{{}^{232}\text{Th}} \right)_0 = 1.5 \pm 50\%$ (second column) and
 473 corrected ages using stratigraphic constraints (third column, see text for detail s). $\delta^{234}\text{U}_i$ is the $\delta^{234}\text{U}$ at
 474 initial time (using ${}^{230}\text{Th}/{}^{234}\text{U}$ ages). Uncertainties are given at 2σ 7

475 Table 3: Mean concentrations (in ppm) in the stalagmite, the bedrock, and the soil for each element.
 476 Here, REE are not normalized to the NASC values in order to compare REE data and illustrate the
 477 strong REE enrichment in soils and the low contents in the stalagmite. NA: not analyzed. 11
 478

479

480 REFERENCES:

481 Allen, J. R. M., & Huntley, B. (2000). Weichselian palynological records from southern
 482 Europe : correlation and chronology, *Quaternary International*, 73, 111-125.

483 Baldini, J. U., McDermott, F., Baldini, L. M., Ottley, C. J., Linge, K. L., Clipson, N., & Jarvis, K. E.
 484 (2012). Identifying short-term and seasonal trends in cave drip water trace element
 485 concentrations based on a daily-scale automatically collected drip water dataset. *Chemical*
 486 *Geology*, 330, 1-16.

487 Baldini, L. M., McDermott, F., Baldini, J. U. L., Arias, P., Cueto, M., Fairchild, I. J.,
 488 Hoffmann, D.L., Matthey, D. P., Müller, W., Nita, DC., Ontañón, R., Garcíá-Moncó, C.,
 489 & Richards, D. A. (2015). Regional temperature, atmospheric circulation, and sea-ice
 490 variability within the Younger Dryas Event constrained using a speleothem from
 491 northern Iberia. *Earth and Planetary Science Letters*, 419, 101–110.

492 <https://doi.org/10.1016/j.epsl.2015.03.015>

493 Belli, R., Borsato, A., Frisia, S., Drysdale, R., Maas, R., & Greig, A. (2017). Investigating the
494 hydrological significance of stalagmite geochemistry (Mg, Sr) using Sr isotope and
495 particulate element records across the Late Glacial-to-Holocene transition. *Geochimica et*
496 *Cosmochimica Acta*, 199, 247-263.

497 Bourdin, C., Douville, E., & Genty, D. (2011). Alkaline-earth metal and rare-earth element
498 incorporation control by ionic radius and growth rate on a stalagmite from the Chauvet
499 Cave, Southeastern France. *Chemical Geology*, 290(1–2), 1–11.
500 <https://doi.org/10.1016/j.chemgeo.2011.08.006>

501 Bout-Roumazeilles, V., Combourieu-Nebout, N., Desprat, S., Siani, G., Turon, J. L., &
502 Essallami, L. (2013). Tracking atmospheric and riverine terrigenous supplies variability
503 during the last glacial and the Holocene in central Mediterranean. *Climate of the Past* 9,
504 1065-1087

505 Box, M. R., Krom, M. D., Cliff, R., Almogi-Labin, A., Bar-Matthews, M., Ayalon, A., ... &
506 Paterne, M. (2008). Changes in the flux of Saharan dust to the East Mediterranean Sea
507 since the last glacial maximum as observed through Sr-isotope geochemistry.
508 *Mineralogical Magazine*, 72(1), 307-311.

509 Brauer, A., Haug, G. H., Dulski, P., Sigman, D. M., & Negendank, J. F. W. (2008). An abrupt
510 wind shift in western Europe at the onset of the Younger Dryas cold period. *Nature*
511 *Geoscience*, 1(8), 520–523. <https://doi.org/10.1038/ngeo263>

512 Carignan, J., Hild, P., Mevelle, G., Morel, J., & Yeghicheyan, D. (2001). Routine Analyses of
513 trace Elements in Geological Samples using Flow injection and Low Pressure On-Line
514 liquid Chromatography Coupled to ICP-MS: A study of Geochemical Reference
515 Materials BR, DR-N, UB-N, AN-G and GH. *Geostandards Newsletter*, 25(2–3), 187–
516 198. <https://doi.org/10.1111/j.1751-908X.2001.tb00595.x>

517 Carolin, S. A., Walker, R. T., Day, C. C., Ersek, V., Sloan, R. A., Dee, M. W., ... &
518 Henderson, G. M. (2019). Precise timing of abrupt increase in dust activity in the
519 Middle East coincident with 4.2 ka social change. *Proceedings of the National*
520 *Academy of Sciences*, *116*(1), 67-72.

521 Chabaud, L., Sánchez Goñi, M. F., Desprat, S., & Rossignol, L. (2014). Land-sea climatic
522 variability in the eastern North Atlantic subtropical region over the last 14,200 years:
523 Atmospheric and oceanic processes at different timescales. *Holocene*, *24*(7), 787–797.
524 <https://doi.org/10.1177/0959683614530439>

525 Cheng, H., Edwards, R. L., Shen, C. C., Polyak, V. J., Asmerom, Y., Woodhead, J., Hellstrom, J.,
526 Wang, Y., Kong, X., Spötl, C., Wang, X., & Alexander, E.C. (2013). Improvements in ²³⁰Th
527 dating, ²³⁰Th and ²³⁴U half-life values, and U–Th isotopic measurements by multi-collector
528 inductively coupled plasma mass spectrometry. *Earth and Planetary Science Letters*, *371*, 82-91.

529 Cowan, G. A., & Adler, H. H. (1976). The variability of the natural abundance of ²³⁵U.
530 *Geochimica et Cosmochimica Acta*, *40*(12), 1487–1490. [https://doi.org/10.1016/0016-](https://doi.org/10.1016/0016-7037(76)90087-9)
531 [7037\(76\)90087-9](https://doi.org/10.1016/0016-7037(76)90087-9)

532 Elderfield, H., Upstill-Goddard, R., & Sholkovitz, E. R. (1990). The rare earth elements in
533 rivers, estuaries, and coastal seas and their significance to the composition of ocean
534 waters. *Geochimica et Cosmochimica Acta*, *54*(4), 971–991.
535 [https://doi.org/10.1016/0016-7037\(90\)90432-K](https://doi.org/10.1016/0016-7037(90)90432-K)

536 Erel Y., & Torrent, J. (2010). Contribution of Saharan dust to Mediterranean soils assessed by
537 sequential extraction and Pb and Sr isotopes. *Chemical Geology*, *275*(1-2), 19-25.

538 Fairchild, I. J., Borsato, A., Tooth, A. F., Frisia, S., Hawkesworth, C. J., Huang, Y., ... Spiro,
539 B. (2000). Controls on trace element (Sr-Mg) compositions of carbonate cave waters:
540 Implications for speleothem climatic records. *Chemical Geology*, *166*(3–4), 255–269.
541 [https://doi.org/10.1016/S0009-2541\(99\)00216-8](https://doi.org/10.1016/S0009-2541(99)00216-8)

542 Fairchild, I. J., & Treble, P. C. (2009). Trace elements in speleothems as recorders of
543 environmental change. *Quaternary Science Reviews*, 28(5–6), 449–468.
544 <https://doi.org/10.1016/j.quascirev.2008.11.007>

545 Frumkin, A., & Stein, M. (2004). The Sahara-East Mediterranean dust and climate connection
546 revealed by strontium and uranium isotopes in a Jerusalem speleothem. *Earth and
547 Planetary Science Letters*, 217(3–4), 451–464. [https://doi.org/10.1016/S0012-
548 821X\(03\)00589-2](https://doi.org/10.1016/S0012-821X(03)00589-2)

549 García-Ruiz, J. ., Palacios, D., Gonzalez-Samperiz, P., de Andres, N., Moreno, A., Valero-
550 Garces, B., & Gomez-Villar, A. (2016). Mountain glacier evolution in the Iberian
551 Peninsula during the Younger Dryas. *Quaternary Science Reviews*, 138, 16–30.

552 Gascoyne, M. (1983). Trace-element partition coefficients in the calcite-water system and
553 their paleoclimatic significance in cave studies. *Journal of Hydrology*, 61(1–3), 213–222.
554 [https://doi.org/10.1016/0022-1694\(83\)90249-4](https://doi.org/10.1016/0022-1694(83)90249-4)

555 Genty, D., Blamart, D., Ghaleb, B., Plagnes, V., Causse, C., Bakalowicz, M., Zouari, K.,
556 Chkir, N., Hellstrom, J., Wainer, K., & Bourges, F. (2006). Timing and dynamics of the
557 last deglaciation from European and North African $\delta^{13}\text{C}$ stalagmite profiles-comparison
558 with Chinese and South Hemisphere stalagmites. *Quaternary Science Reviews*, 25(17–
559 18), 2118–2142. <https://doi.org/10.1016/j.quascirev.2006.01.030>

560 Goede, A., McCulloch, M., McDermott, F., & Hawkesworth, C. (1998). Aeolian contribution
561 to strontium and strontium isotope variations in a tasmanian speleothem. *Chemical
562 Geology*, 149(1–2), 37–50. [https://doi.org/10.1016/S0009-2541\(98\)00035-7](https://doi.org/10.1016/S0009-2541(98)00035-7)

563 Gromet, L. P., Haskin, L. A., Korotev, R. L., & Dymek, R. F. (1984). The “North American
564 shale composite”: Its compilation, major and trace element characteristics. *Geochimica
565 et Cosmochimica Acta*, 48(12), 2469–2482. [https://doi.org/10.1016/0016-
566 7037\(84\)90298-9](https://doi.org/10.1016/0016-7037(84)90298-9)

567 Guiter, F., Andrieu-Ponel, V., Digerfeldt, G., Reille, M., de Beaulieu, J-L., & Ponel, P.
568 (2005). Vegetation history and lake-level changes from the Younger Dryas to the present in
569 Eastern Pyrenees (France): pollen, plant macrofossils and lithostratigraphy from Lake
570 Racou (2000 m a. s. l.), *Vegetation History and Archaeobotany* 14 (99–118).
571 <https://doi.org/10.1007/s00334-005-0065-z>

572 Han, C., Do Hur, S., Han, Y., Lee, K., Hong, S., Erhardt, T., Fischer, H., Svensson, A.M.,
573 Steffensen, J.P. and Vallelonga, P., 2018. High-resolution isotopic evidence for a
574 potential Saharan provenance of Greenland glacial dust. *Scientific reports*, 8.

575 Harding, D. J., Arden, J. W., & Rickaby, R. E. M. (2006). A method for precise analysis of
576 trace element/calcium ratios in carbonate samples using quadrupole inductively coupled
577 plasma mass spectrometry. *Geochemistry, Geophysics, Geosystems*, 7(6).
578 <https://doi.org/10.1029/2005GC001093>

579 Hartland, A., Fairchild, I. J., Lead, J. R., Borsato, A., Baker, A., Frisia, S., & Baalousha, M.
580 (2012). From soil to cave: Transport of trace metals by natural organic matter in karst
581 dripwaters. *Chemical Geology*, 304–305, 68–82.
582 <https://doi.org/10.1016/j.chemgeo.2012.01.032>

583 Heiri, O., & Millet, L. (2005). Reconstruction of Late Glacial summer temperatures from
584 chironomid assemblages in Lac Lautrey (Jura, France), *Journal of Quaternary Science*,
585 20, 33–44. <https://doi.org/10.1002/jqs.895>

586 Hellstrom, J. (2006). U–Th dating of speleothems with high initial ²³⁰Th using stratigraphical
587 constraint. *Quaternary Geochronology*, 289–295.
588 <https://doi.org/10.1016/j.quageo.2007.01.004>

589 Hellstrom, J. C., & McCulloch, M. T. (2000). Multi-proxy constraints on the climatic
590 significance of trace element records from a New Zealand speleothem. *Earth and*
591 *Planetary Science Letters*, 179(2), 287–297. <https://doi.org/10.1016/S0012->

- 593 Hercman, H., & Pawlak, J. (2012). MOD-AGE: An age-depth model construction algorithm.
594 *Quaternary Geochronology*, 12, 1–10. <https://doi.org/10.1016/j.quageo.2012.05.003>
- 595 Kasper, K., Van der Meer, M. T. J. Mets, A., Zahn, R., Sinninghe Damsté, J.S., & Schouten,
596 S. (2014). Salinity changes in the Agulhas leakage area recorded by stable hydrogen
597 isotopes of C 37 alkenones during Termination I and II, *Climate of the Past*, 10 (251–
598 260). <https://doi.org/10.5194/cp-10-251-2014>
- 599 Kisakürek, B., Widdowson, M., & James, R. H. (2004). Behaviour of Li isotopes during
600 continental weathering: The Bidar laterite profile, India. *Chemical Geology*, 212(1–2),
601 27–44. <https://doi.org/10.1016/j.chemgeo.2004.08.027>
- 602 Lotter Eawag. (1992). Late-glacial climatic oscillations as recorded in Swiss lake sediments.
603 *Journal of Quaternary Science*, 7(1992), 187–204.
- 604 Magny, M. (2001). Palaeohydrological changes as reflected by lake-level fluctuations in the
605 Swiss Plateau, the Jura Mountains and the northern French Pre-Alps during the Last
606 Glacial – Holocene transition : a regional synthesis. *Global and Planetary Change*, 30,
607 85-101.
- 608 Magny, M., Aalbersberg, G., Bégeot, C., Benoit-ruffaldi, P., Bossuet, G., Disnar, J.R., Heiri,
609 O., Laggoun-Defarge, F., Mazier, F., Millet, L., Peyron, O., Vannière, B., & Walter-
610 Simonnet, A.V. (2006). Environmental and climatic changes in the Jura mountains
611 (eastern France) during the Lateglacial – Holocene transition: a multi-proxy record from
612 Lake Lautrey, *Quaternary Science Reviews*, 25(5-6), 414–445.
613 <https://doi.org/10.1016/j.quascirev.2005.02.005>
- 614 Magny, M., Combourieu-Nebout, N., De Beaulieu, J. L., Bout-Roumazeilles, V.,
615 Colombaroli, D., Desprat, S., Francke, A., Joannin, S., Ortu, E., Peyron, O., Revel, M.,
616 Sadori, L., Siani, G., Sicre, M. A., Samartin, S., Simonneau, A., Tinner, W., Vannière,

617 B., Wagner, B., Zanchetta, G., Anselmetti, F., Brugiapaglia, E., Chapron, E., Debret, M.,
618 Desmet, M., Didier, J., Essallami, L., Galop, D., Gilli, A., Haas, J. N., Kallel, N., Millet,
619 L., Stock, A., Turon, J. L., & Wirth, S. (2013). North-south palaeohydrological contrasts
620 in the central mediterranean during the holocene: Tentative synthesis and working
621 hypotheses. *Climate of the Past*, 9(2043–2071). <https://doi.org/10.5194/cp-9-2043-2013>

622 Magny, M., Vannière, B., de Beaulieu, J. L., Bégeot, C., Heiri, O., Millet, L., Peyron, O., &
623 Walter-Simonnet, A. V. (2007). Early-Holocene climatic oscillations recorded by lake-
624 level fluctuations in west-central Europe and in central Italy. *Quaternary Science*
625 *Reviews*, 26(15–16), 1951–1964. <https://doi.org/10.1016/j.quascirev.2006.04.013>

626 Merino E. and Banerjee A. (2008) "Terra Rossa Genesis, Implications for Karst, and Eolian
627 Dust: A Geodynamic Thread," *The Journal of Geology* 116 (1): 62-75.

628 Millot, R., Vigier, N., & Gaillardet, J. (2010). Behaviour of lithium and its isotopes during
629 weathering in the Mackenzie Basin, Canada. *Geochimica et Cosmochimica Acta*, 74(14),
630 3897–3912. <https://doi.org/10.1016/j.gca.2010.04.025>

631 Moreno, A., & Palacios, D. (2016). Mountain glacier evolution in the Iberian Peninsula
632 during the Younger Dryas, *Quaternary Science Reviews*, 138 (16-30).
633 <https://doi.org/10.1016/j.quascirev.2016.02.022>

634 Moreno, A., Stoll, H., Cacho, I., Valero-garcés, B., Ito, E., & Edwards, R. L. (2010). A
635 speleothem record of glacial (25 – 11 . 6 kyr BP) rapid climatic changes from northern
636 Iberian Peninsula. *Global and Planetary Change*, 71(3–4), 218–231.
637 <https://doi.org/10.1016/j.gloplacha.2009.10.002>

638 Muhs, D. R., Budahn, J. R., Prospero, J. M., & Carey, S. N. (2007). Geochemical evidence for
639 African dust inputs to soils of western Atlantic islands: Barbados, the Bahamas, and
640 Florida. *Journal of Geophysical Research: Earth Surface*, 112(F2).

641 Neugebauer, I., Brauer, A., Dräger, N., Dulski, P., Wulf, S., Plessen, B., Mingram, J.,

642 Herzs Schuh, U., & Brande, A. (2012). A Younger Dryas varve chronology from the
643 Rehwise palaeolake record in NE-Germany. *Quaternary Science Reviews*, 36, 91–102.
644 <https://doi.org/10.1016/j.quascirev.2011.12.010>

645 Owen, R.A., Day, C.C., Hu, C.-Y., Liu, Y.-H., Pointing, M.D., Blättler, C.L., & Henderson,
646 G.M. (2016). Calcium isotopes in caves as a proxy for aridity: Modern calibration and
647 application to the 8.2 kyr event. *Earth and Planetary Science Letters*, 443, 129–138.
648 <http://dx.doi.org/10.1016/j.epsl.2016.03.027>

649 Palmer, M. R., & Edmond, J. M. (1989). Cesium and rubidium in submarine hydrothermal
650 fluids: evidence for recycling of alkali elements. *Earth and Planetary Science Letters*,
651 95(1–2), 8–14. [https://doi.org/10.1016/0012-821X\(89\)90163-5](https://doi.org/10.1016/0012-821X(89)90163-5)

652 Pazand, K., & Javanshir, A. R. (2013). Rare earth element geochemistry of spring water,
653 north western Bam, NE Iran. *Applied Water Science*, 4(1), 1–9.
654 <https://doi.org/10.1007/s13201-013-0125-y>

655 Pons-Branchu, E., Hamelin, B., Brulhet, J., & Bruxelles, L. (2004). Speleothem rupture in
656 karst: Tectonic or climatic origin? U-Th dating of rupture events in Salamandre Cave
657 (Gard, southeastern France). *Bulletin de La Societe Geologique de France*, 175(5), 473–
658 479. <https://doi.org/10.2113/175.5.473>

659 Pons-Branchu E., Douville E., Roy-Barman M., Dumont E., Branchu E., Thil F., Frank N.,
660 Bordier L. and Borst W. (2014). A geochemical perspective on Parisian urban history
661 based on U-Th dating, laminae counting and yttrium and REE concentrations of recent
662 carbonates in underground aqueducts. *Quaternary Geochronology* 24, 44-53.

663 Pourret, O., Davranche, M., Gruau, G., & Dia, A. (2008). New insights into cerium anomalies
664 in organic-rich alkaline waters. *Chemical Geology*, 251(1–4), 120–127.
665 <https://doi.org/10.1016/j.chemgeo.2008.03.002>

- 666 Richter, D. K., Gotte, T., Niggemann, S., Wurth, G., & Bochum, D.-. (2004). REE³⁺ and
667 Mn²⁺ cathodoluminescence in lateglacial and Holocene stalagmites of central Europe :
668 evidence for climatic processes ?, *The Holocene*, *14*, 759–767.
- 669 Riedel, T., & Kübeck, C. (2018). Uranium in groundwater – A synopsis based on a large
670 hydrogeochemical data set. *Water Research*, *129*, 29–38.
671 <https://doi.org/10.1016/j.watres.2017.11.001>
- 672 Roberts, M. S., Smart, P. L., & Baker, A. (1998). Annual trace element variations in a
673 Holocene speleothem. *Earth and Planetary Science Letters*, *154*(1-4), 237-246.
- 674 Rodrigo-Gámiz, M., Martínez-Ruiz, F., Jiménez-Espejo, F. J., Gallego-Torres, D.,
675 Nieto-Moreno, V., Romero, O., & Ariztegui, D. (2011). Impact of climate variability in
676 the western Mediterranean during the last 20,000 years: oceanic and atmospheric
677 responses. *Quaternary Science Reviews*, *30*(15-16), 2018-2034.
- 678 Rosenthal, Y., Field, M.P., & Sherrell, R. M. (1999). Precise determination of
679 element/calcium ratios in calcareous samples using sector field inductively coupled
680 plasma mass spectrometry. *Analytical Chemistry*, *71*(15), 3248.
- 681 Roy-Barman, M., & Pons-Branchu, E. (2016). Improved U–Th dating of carbonates with high initial
682 ²³⁰Th using stratigraphical and coevality constraints. *Quaternary Geochronology*, *32*, 29-39.
- 683 Rutledge, H., Baker, A., Marjo, C. E., Andersen, M. S., Graham, P. W., Cuthbert, M. O., Rau,
684 G. C., Roshan, H., Markowska, M., Mariethoz, G., & Jex, C. N. (2014). Dripwater
685 organic matter and trace element geochemistry in a semi-arid karst environment :
686 Implications for speleothem paleoclimatology. *Geochimica et Cosmochimica Acta*, *135*,
687 217–230. <https://doi.org/10.1016/j.gca.2014.03.036>
- 688 Schimpf, D., Kilian, R., Kronz, A., Simon, K., Spötl, C., Wörner, G., Deininger, M., &
689 Mangini, A. (2011). The significance of chemical, isotopic, and detrital components in

690 three coeval stalagmites from the superhumid southernmost Andes (53°S) as high-
691 resolution palaeo-climate proxies. *Quaternary Science Reviews*, 30(3–4), 443–459.
692 <https://doi.org/10.1016/j.quascirev.2010.12.006>

693 Severinghaus, J. P., Sowers, T., Brook, E. J., Alley, R. B., & Bender, M. L. (1998). Timing of
694 abrupt climate change at the end of the Younger Dryas interval from thermally
695 fractionated gases in polar ice, *Nature*, 391, 141.

696 Sholkovitz, E. R. (1992). Chemical evolution of rare earth elements: fractionation between
697 colloidal and solution phases of filtered river water. *Earth and Planetary Science Letters*,
698 114(1), 77–84. [https://doi.org/10.1016/0012-821X\(92\)90152-L](https://doi.org/10.1016/0012-821X(92)90152-L)

699 Tanaka, K., & Watanabe, N. (2015). Size distribution of alkali elements in riverbed sediment
700 and its relevance to fractionation of alkali elements during chemical weathering.
701 *Chemical Geology*, 411, 12–18. <https://doi.org/10.1016/j.chemgeo.2015.05.025>

702 Tanizaki, Y., Shimokawa, T., & Yamazaki, M.. (1992). Physico-chemical speciation of trace
703 elements in urban streams by size fractionation, *Water Research*, 26, 55–63.

704 Ünal-Imer, E., Shulmeister, J., Zhao, J. X., Uysal, I. T., & Feng, Y. X. (2016). High-
705 resolution trace element and stable/radiogenic isotope profiles of late Pleistocene to
706 Holocene speleothems from Dim Cave, SW Turkey. *Palaeogeography*,
707 *Palaeoclimatology*, *Palaeoecology*, 452, 68–79.
708 <https://doi.org/10.1016/j.palaeo.2016.04.015>

709 Vanni re, B., Bossuet, G., Walter-Simonnet, A. V., Ruffaldi, P., Adatte, T., Rossy, M., &
710 Magny, M. (2004). High-resolution record of environmental changes and
711 tephrochronological markers of the Last Glacial-Holocene transition at Lake Lautrey
712 (Jura, France). *Journal of Quaternary Science*, 19(8), 797–808.
713 <https://doi.org/10.1002/jqs.873>

714 von Strandmann, P. A. P., Vaks, A., Bar-Matthews, M., Ayalon, A., Jacob, E., & Henderson, G. M.

- 715 (2017). Lithium isotopes in speleothems: Temperature-controlled variation in silicate weathering
716 during glacial cycles. *Earth and Planetary Science Letters*, 469, 64-74.
- 717 Yang, C., Niu, D., Zhong, Y., Li, L., Lv, H., & Liu, Y. (2018). Adsorption of uranium by
718 hydrous manganese dioxide from aqueous solution. *Journal of Radioanalytical and*
719 *Nuclear Chemistry*, 315(3), 533–542. <https://doi.org/10.1007/s10967-018-5705-8>
- 720 Zhou, H., Greig, A., Tang, J., You, C.-F., Yuan, D., Tong, X., & Huang, Y. (2012). Rare earth
721 element patterns in a Chinese stalagmite controlled by sources and scavenging from karst
722 groundwater. *Geochimica et Cosmochimica Acta*, 83, 1–18.
723 <https://doi.org/10.1016/j.gca.2011.12.027>
- 724 Zhou, H., Wang, Q., Zhao, J., Zheng, L., Guan, H., Feng, Y., & Greig, A. (2008). Rare earth
725 elements and yttrium in a stalagmite from Central China and potential paleoclimatic
726 implications. *Palaeogeography, Palaeoclimatology, Palaeoecology*, 270(1–2), 128–138.
727 <https://doi.org/http://dx.doi.org/10.1016/j.palaeo.2008.09.001>

728

729

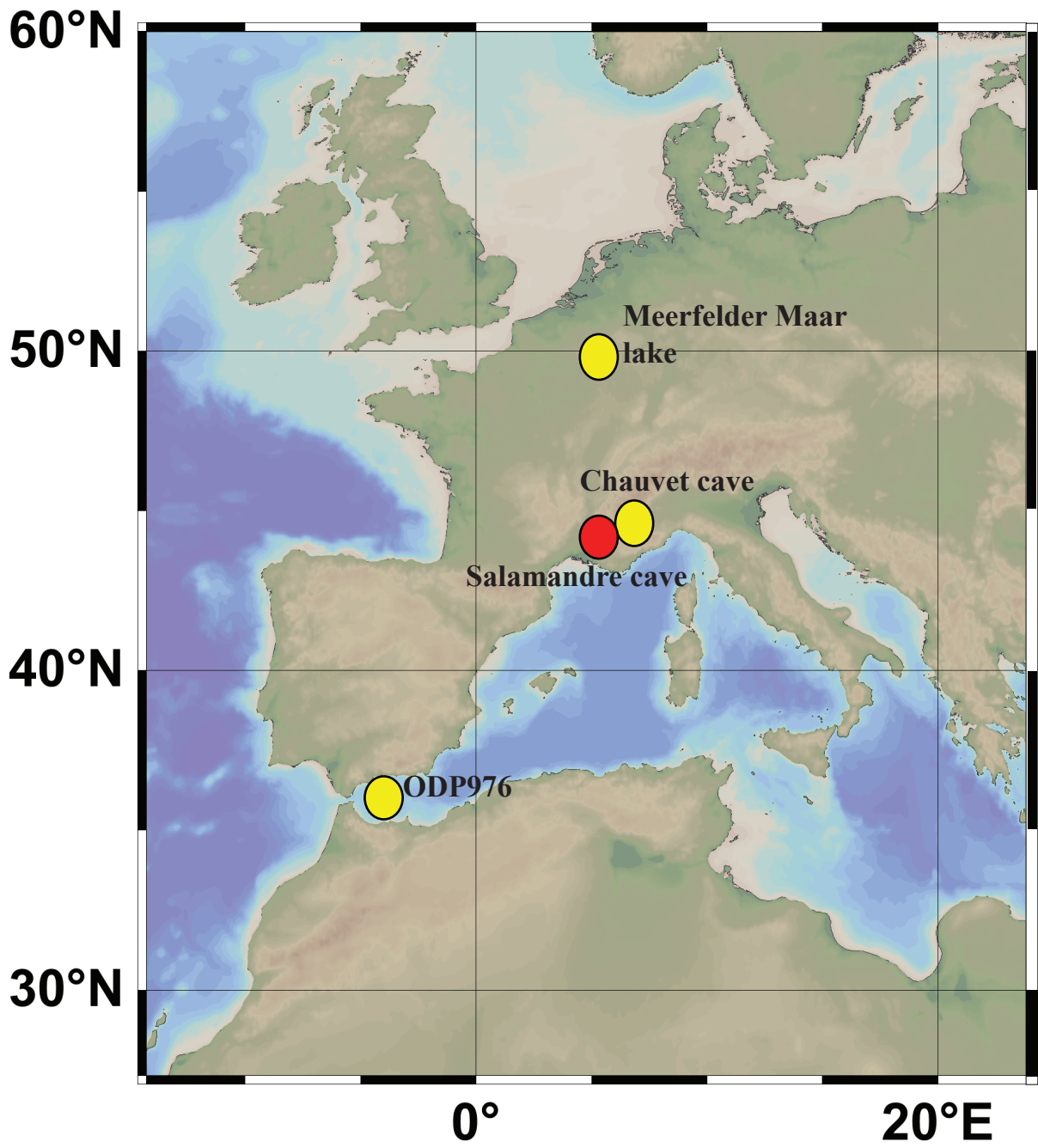
730 **SUPPLEMENTARY MATERIAL**

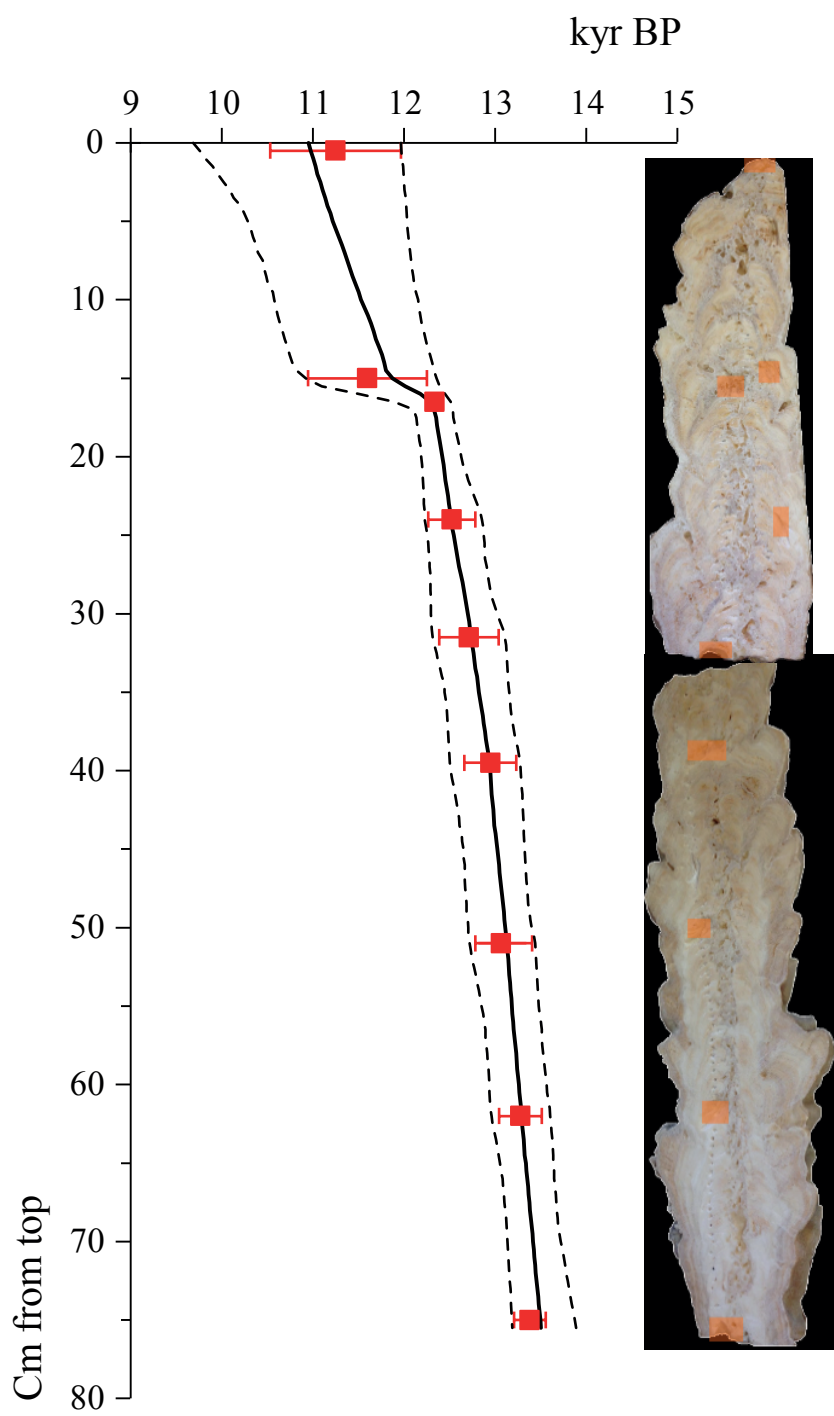
731 Appendix A.

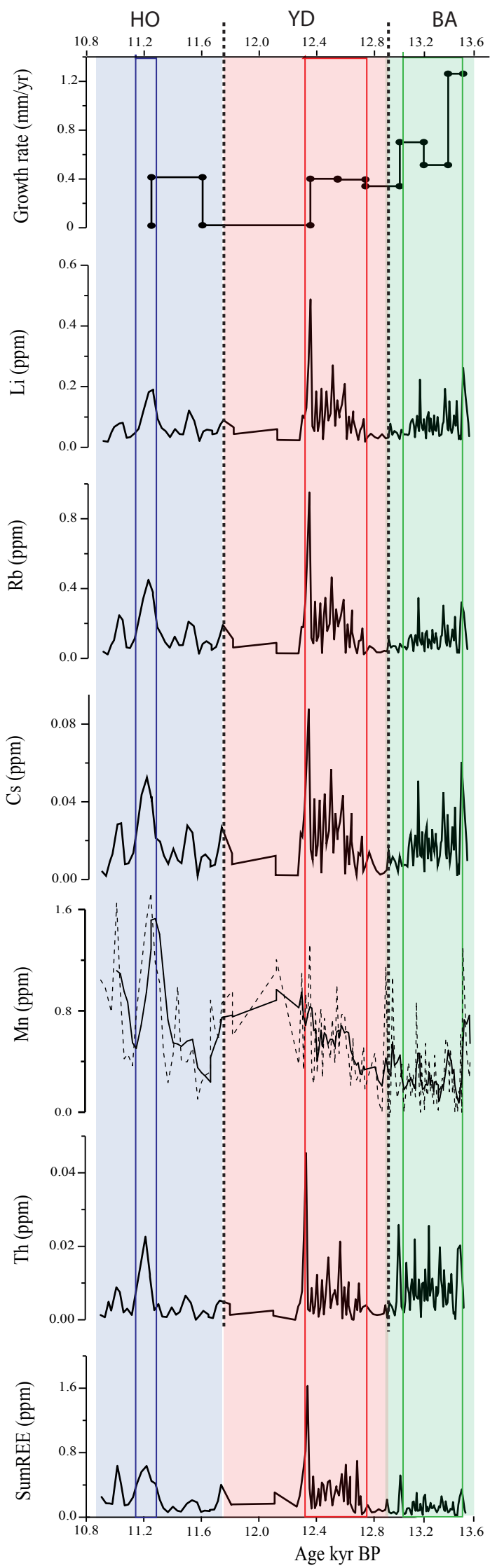
732 A1a: Relation between Cs vs Li

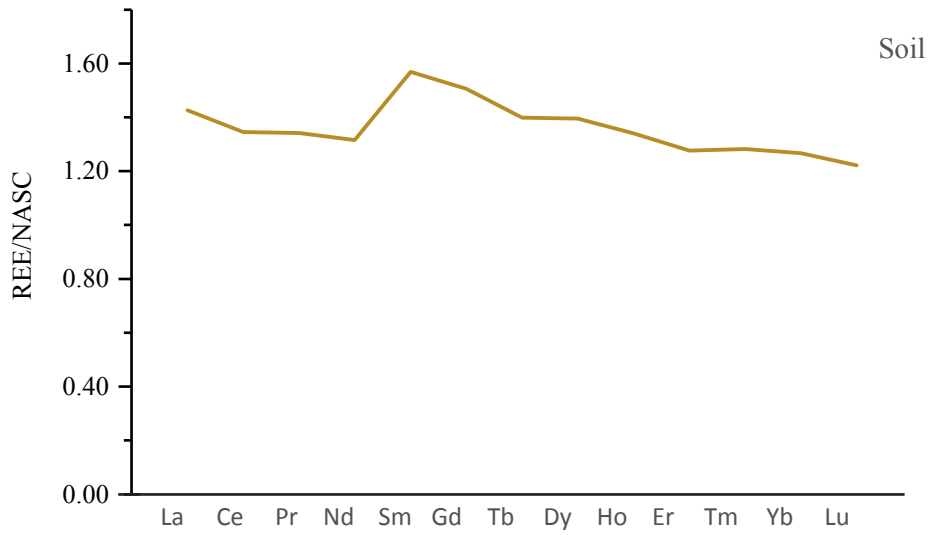
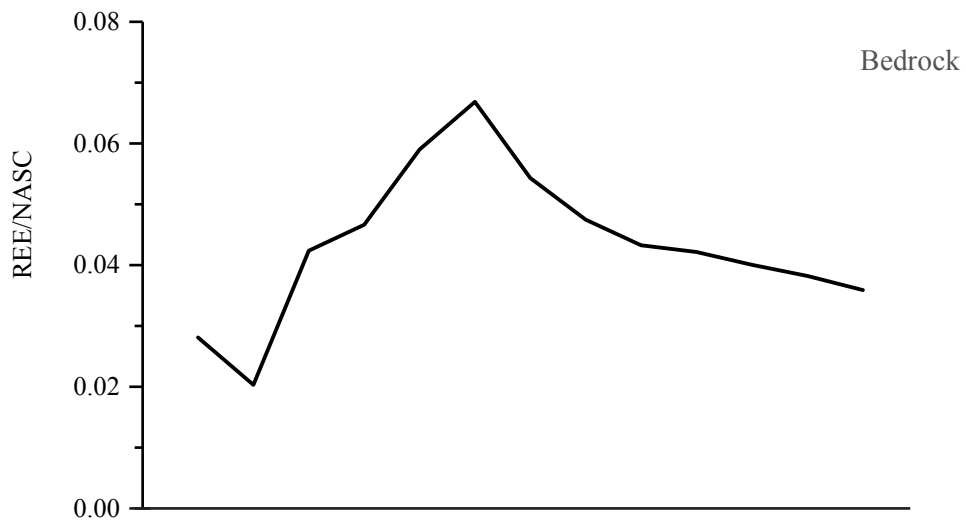
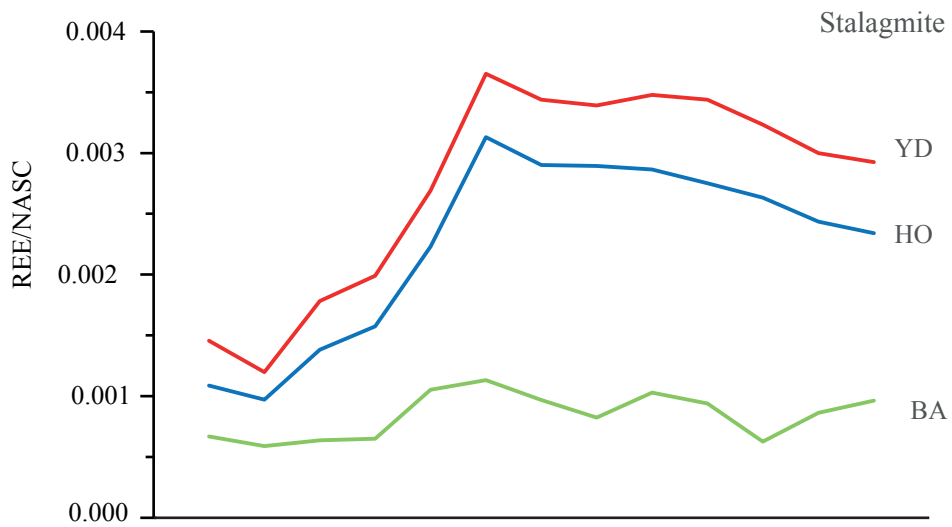
733 A1b: Rb vs Li

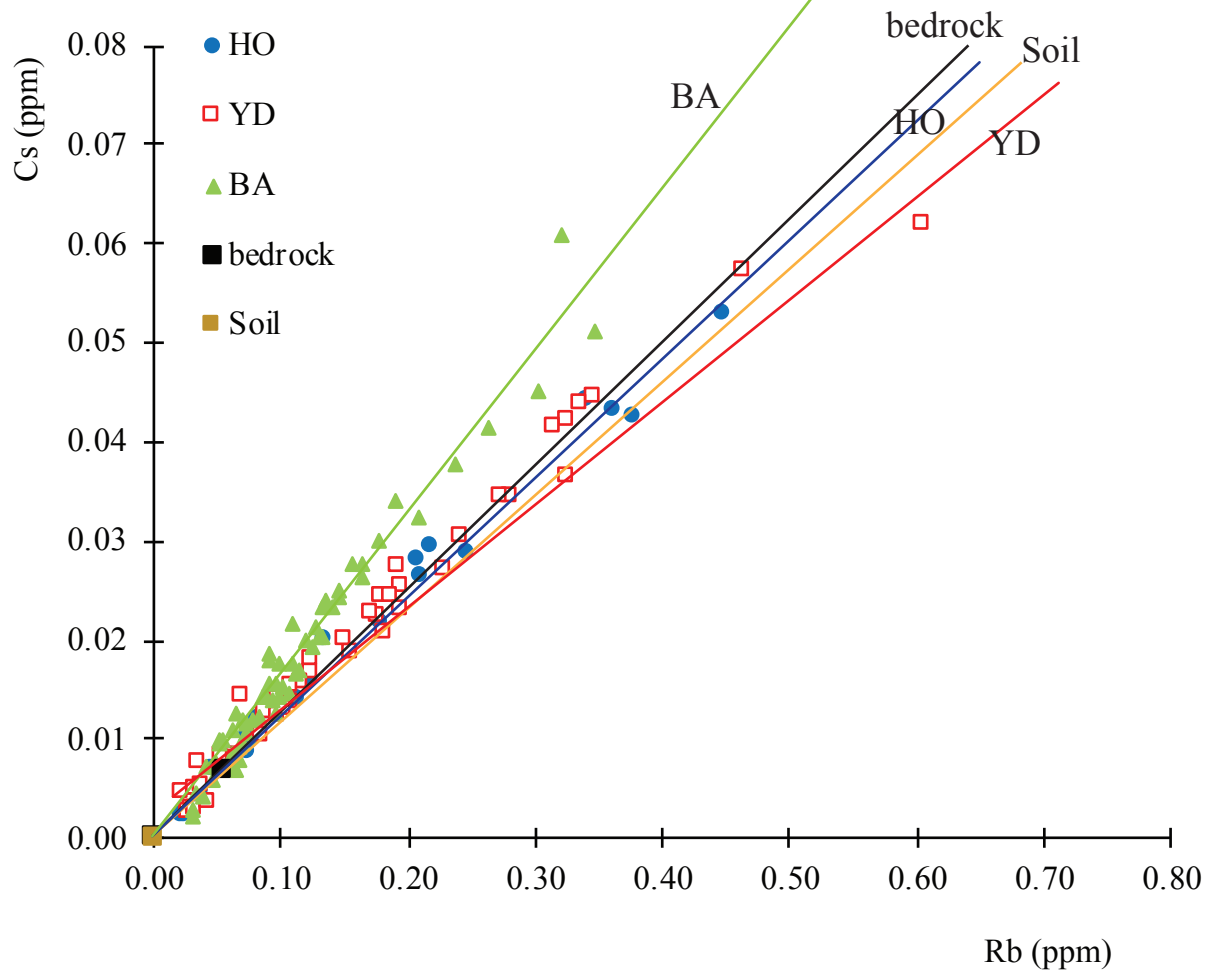
734 A1c: Cs vs Th

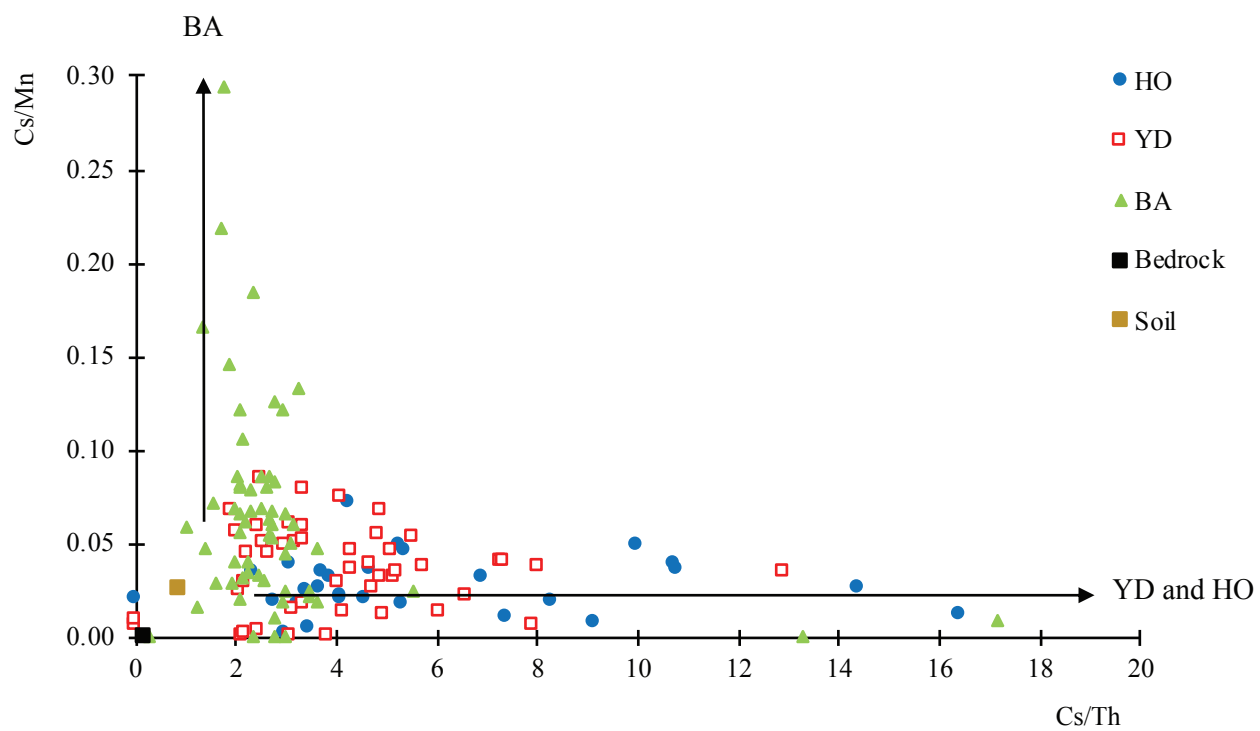


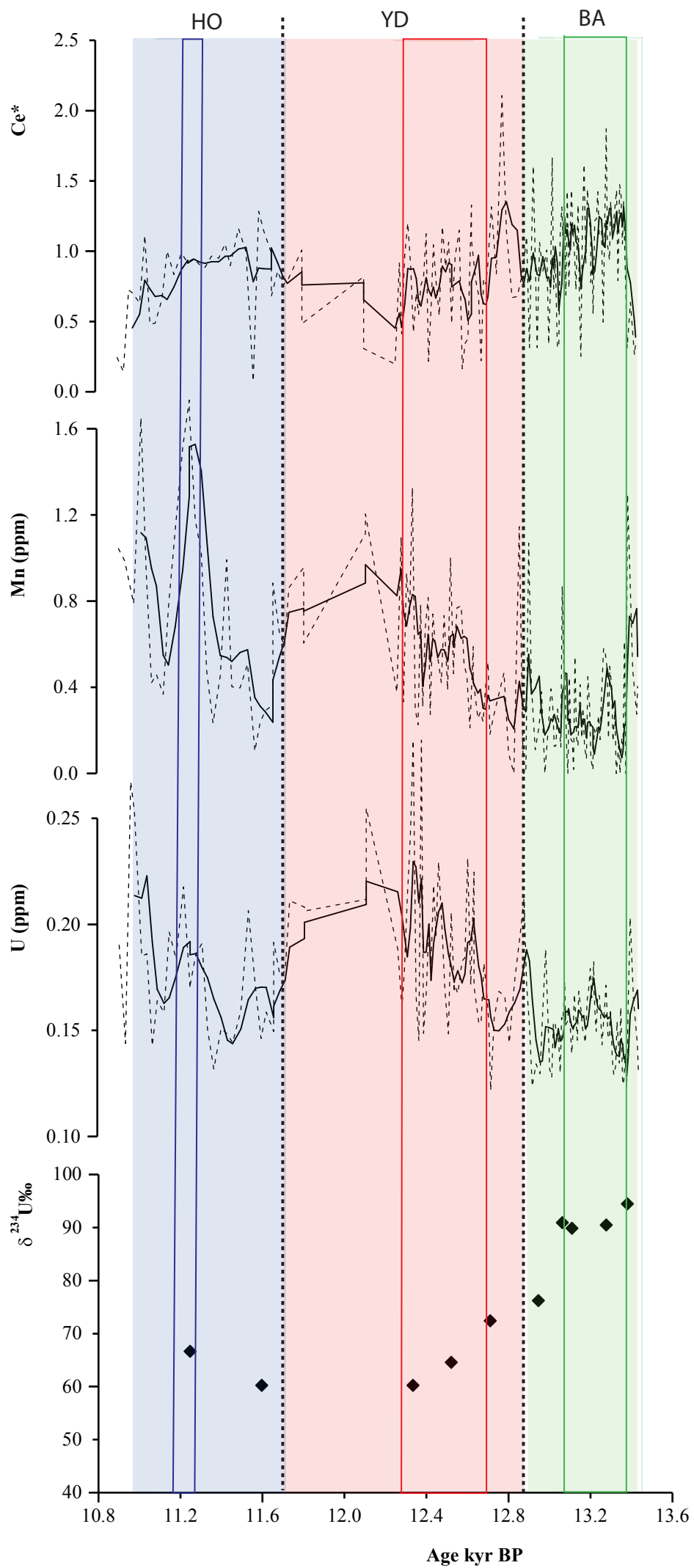












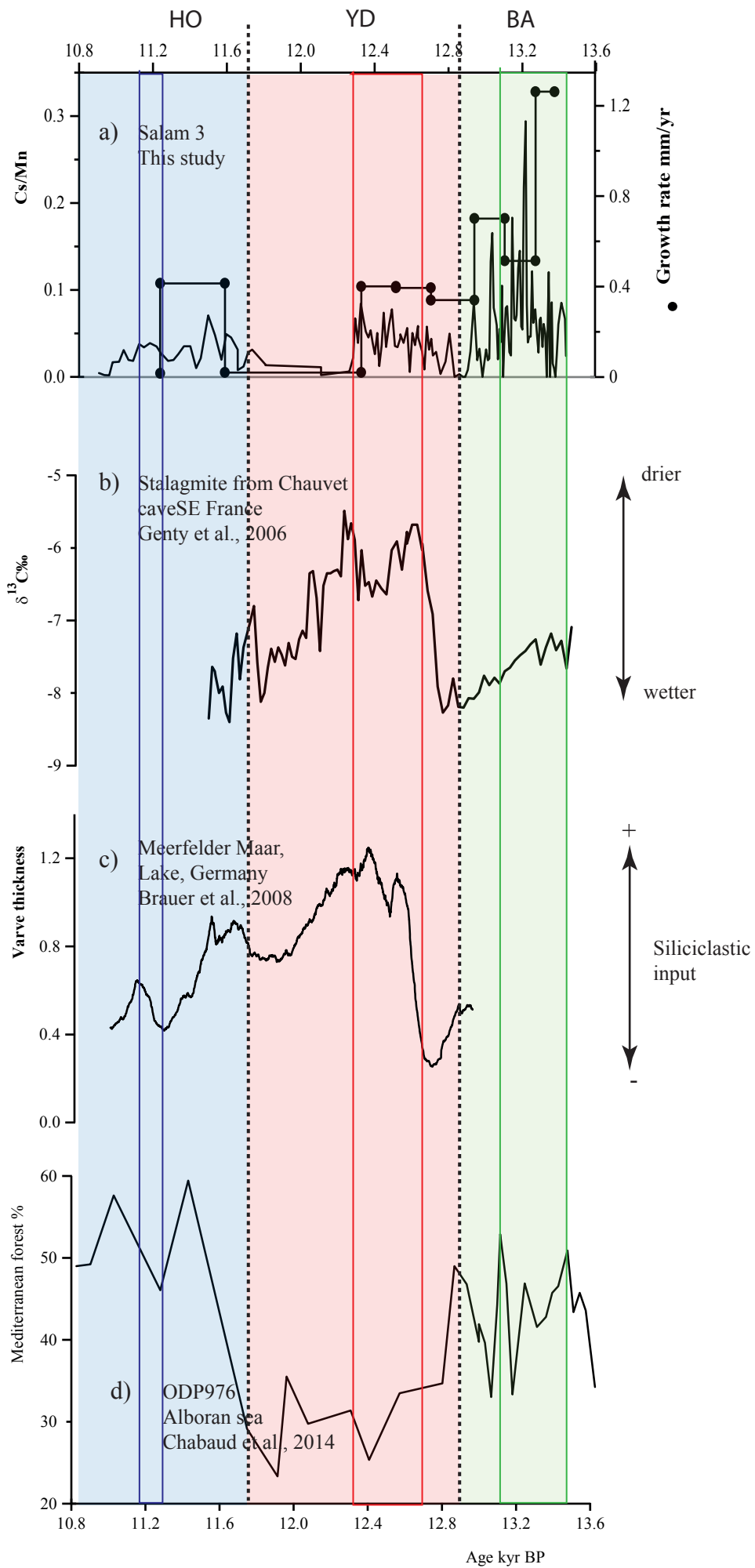


Table 1: Uranium, Thorium concentrations and isotopic ratios. Uncertainties are given at 2σ . $\delta^{234}U_m = ((^{234}U/^{238}U)_{measured}/(^{234}U/^{238}U)_{equilibrium} - 1) \times 1000$, with $^{234}U/^{238}U_{equilibrium} = 54.89 \times 10^{-6}$ (molar ratio, Cheng et al., 2013).

Cm from top	[²³⁸ U] ppm	(±)	[²³² Th] ppb	(±)	(²³⁰ Th/ ²³⁸ U)	(±)	(²³⁰ Th/ ²³² Th)	(±)	$\delta^{234}U_m$ (‰)	(±)
0.5	0.167	0.0013	17.09	0.140	0.152	5.96E-04	4.55	0.02	64.65	0.89
15	0.152	0.0012	16.08	0.140	0.152	1.48E-03	4.36	0.04	58.29	2.44
16.5	0.180	0.0014	1.302	0.010	0.116	7.59E-04	48.9	0.32	58.17	1.40
24	0.136	0.0011	7.584	0.011	0.140	1.30E-03	7.59	0.07	62.3	1.29
31.5	0.164	0.0013	16.49	0.153	0.159	9.25E-04	5.01	0.03	69.82	0.92
39.5	0.162	0.0013	7.699	0.062	0.142	6.98E-04	9.13	0.04	73.47	1.00
51	0.169	0.0014	11.30	0.143	0.153	2.50E-03	6.94	0.03	86.58	1.02
51	0.152	0.0012	7.952	0.064	0.145	5.02E-04	8.47	0.03	87.61	0.98
62	0.141	0.0011	8.939	0.087	0.152	1.26E-03	7.66	0.06	87.10	0.76
75	0.154	0.0012	3.372	0.030	0.135	7.87E-04	19.6	0.11	90.91	1.37

Table 2: ²³⁰Th/²³⁴U ages for Salam3 stalagmite. Ages are expressed in kyr BP (before 1950). Uncorrected ages (first column), corrected ages using (²³⁰Th/²³²Th)₀ = 1.5 ± 50% (second column) and corrected ages using stratigraphic constraints (third column, see text for detail s). $\delta^{234}U_i$ is the $\delta^{234}U$ at initial time (using ²³⁰Th/²³⁴U ages). Uncertainties are given at 2σ

Cm from top	Uncorrected ages (kyr BP)		Corrected ages 1 (kyr BP)		Corrected ages 2 (kyr BP)		$\delta^{234}U_i$	
	age	(±)	age	(±)	age	(±)	(‰)	(±)
0.5	16.70	0.09	11.73	2.52	11.25	0.72	66.63	0.92
15	16.87	0.22	11.65	2.77	11.60	0.65	60.23	2.52
16.5	12.65	0.11	12.29	0.29	12.33	0.09	60.23	1.45
24	15.34	0.17	12.55	1.55	12.52	0.26	64.54	1.33
31.5	17.42	0.13	12.72	2.43	12.71	0.33	72.37	0.96
39.5	15.46	0.10	13.12	1.26	12.95	0.29	76.21	1.04
51	16.45	0.31	13.21	1.90	13.11	0.30	89.85	1.07
51	15.62	0.07	12.96	1.32	13.06	0.28	90.90	0.98
62	16.40	0.16	13.47	1.61	13.28	0.23	90.43	0.79
75	14.31	0.11	13.42	0.62	13.38	0.17	94.42	1.42

Table 3: Mean concentrations (in ppm) in the stalagmite, the bedrock, and the soil for each element. Here, REE are not normalized to the NASC values in order to compare REE data and illustrate the strong REE enrichment in soils and the low contents in the stalagmite. NA: not analyzed.

ppm	Li	Mn	Rb	Sr	Y	Cs	La	Lu	Th	U
Stalagmite	0.091	0.54	0.14	15.38	0.094	0.019	0.039	0.0010	0.0068	0.17
Bedrock	0.042	31.90	0.055	92.59	0.87	0.0067	1.07	0.016	0.16	1.54
Soil	NA	649.28	146.73	91.27	36.89	16.46	54.48	0.54	18.72	3.96